

End-to-End Waveform and Beamforming Optimization for RF Wireless Power Transfer

Abdul Basit Khattak, Onel L. A. López, Amirhossein Azarbahram, Deepak Kumar, Matti Latva-aho
Centre for Wireless Communications (CWC), University of Oulu, Finland
Emails: {abdul.khattak, onel.alcarazlopez, amirhossein.azarbahram, deepak.kumar, matti.latva-aho}@oulu.fi

Abstract—Radio frequency (RF) wireless power transfer (WPT) is a key technology for future low-power wireless systems. However, the inherently low end-to-end power transfer efficiency (PTE) is challenging for practical applications. The main factors contributing to it are the channel losses, transceivers' power consumption, and losses related, e.g., to the digital-to-analog converter (DAC), high-power amplifier, and rectenna. Optimizing PTE requires careful consideration of these factors, motivating the current work. Herein, we consider an analog multi-antenna power transmitter that aims to charge a single energy harvester. We first provide a mathematical framework to calculate the harvested power from multi-tone signal transmissions and the system power consumption. Then, we formulate the joint waveform and analog beamforming design problem to minimize power consumption and meet the charging requirements. Finally, we propose an optimization approach relying on swarm intelligence to solve the specified problem. Simulation results quantify the power consumption reduction as the DAC, phase shifters resolution, and antenna length are increased, while it is seen that increasing system frequency results in higher power consumption.

Index Terms—Radio frequency wireless power transfer, power transfer efficiency, waveform optimization, energy beamforming.

I. INTRODUCTION

Wired charging and battery replacements hinder sustainable connectivity in industrial Internet of Things (IoT) installations. Moreover, battery-powered solutions for IoT devices face limitations due to short battery lives and replacement challenges, which are neither cost-effective nor environmentally friendly due to their associated waste. Thus, the research community has focused on energy harvesting (EH) methods as a promising solution to recharge batteries externally, which prevents maintenance and replacements [1], [2].

EH sources can be categorized into ambient, i.e., energy readily available in the environment, and dedicated, i.e., deliberate energy transmissions. The latter category is facilitated by wireless power transfer (WPT) technologies, e.g., inductive coupling, magnetic resonance coupling, laser power beaming, and radiative radio frequency (RF). In contrast to other methods, RF-WPT offers inherent advantages like compact energy receiver (ER) designs, multiuser support, and greater charging radii [3]. Note that RF-EH/WPT are essential enablers of backscattering systems, providing them with the necessary power autonomy, extended range, and environmental sustainability required for diverse IoT and RFID applications. However, its low power transfer efficiency (PTE) is a critical challenge that needs to be carefully addressed [1], [4].

Recent research has focused on waveform design, beamforming optimization, and link-level assessments to improve the efficiency of RF-WPT systems, e.g., [5]–[7]. Notice that proper waveform can enhance the PTE by leveraging the non-linear behavior of the system's key components, e.g., rectenna and high power amplifier (HPA). Specifically, it is shown that utilizing a high peak-to-average power ratio

signal can improve the rectenna's RF-to-direct current (DC) conversion efficiency [8]. Meanwhile, energy beamforming (EB) can be used to focus the RF signal toward the ER to compensate for the channel losses, thereby, enhancing the amount of available RF power for EH purposes [7]. Note that EB flexibility and potential gains are determined by the transmitter architecture, which significantly impacts the power consumption of RF-WPT systems [9]. In a fully-digital architecture, each transmitting antenna requires a dedicated RF chain, with its corresponding HPA. Moreover, the HPA's signal amplification requires a DC power source, which accounts for the majority of the system's power consumption. Notably, the HPA introduces non-linear signal distortion that requires precise modeling [10]. The digital-to-analog converter (DAC) is another crucial component with its cost and power consumption scaling with the resolution and sampling rate [11]. Overall, the high complexity and cost associated with fully-digital structures make it impractical for applications requiring massive implementations [12]. Meanwhile, the analog counterpart is a simpler architecture as it can operate with a single RF chain at the cost of single beam transmissions and less spatial flexibility. Moreover, the analog beamforming reduces the power transmitter (PT) energy consumption, hardware complexity, and the overall deployment cost [13].

In this paper, we consider a multi-antenna analog RF-WPT system comprising multiple phase shifters (PSs) with a limited resolution to promote low-cost implementations. Also, we consider a near-field wireless channel to emphasize the role of near-field WPT systems [2]. Our contributions are:

- We consider the main non-linear components of the system, e.g., HPA and rectenna. Although the authors in [14] consider these non-linearities, our EH model is a generic model [6] based on circuit analysis that accurately captures the EH nonlinearity without relying on Taylor approximation as in [14], [15]. Additionally, we derive the closed-form expression for the DC output voltage.
- We formulate a joint waveform and beamforming design problem aiming to minimize a single-ER system's power consumption and meet the EH requirements. This differs from [14], [16], [17], which focused on increasing the harvested power given a transmit power. Additionally, fully-digital and hybrid architectures are considered in [14], [18], but herein, we consider an analog architecture with limited resolution. Note that the complexities associated with the HPA modeling, the EH model, and the limited-resolution phase shifts make the existing optimization frameworks for RF-WPT systems inapplicable to our system, which calls for novel solutions.
- We propose an optimization approach relying on particle swarm optimization (PSO) to solve the joint waveform and beamforming design problem. This is done by incorporating the user's harvesting DC power requirements in the objective function of the optimization problem, thus compelling the algorithm to discover a feasible solution before minimizing the power consumption. Hereby, we

This work is partially supported in Finland by the Finnish Foundation for Technology Promotion, the Research Council of Finland (Grants 348515 and 346208 (6G Flagship)) and by the European Commission through the Horizon Europe/JU SNS project Hexa-X-II (Grant Agreement no. 101095759)

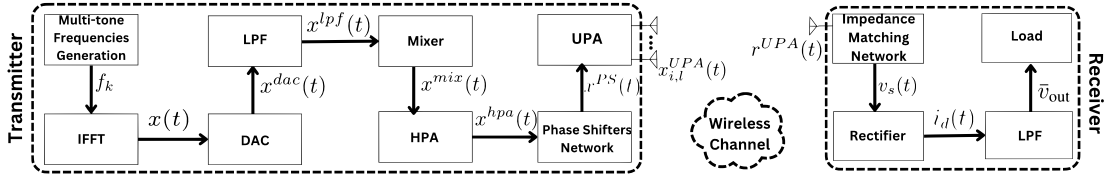


Fig. 1: Block diagram of the proposed RF-WPT system.

cope with the non-convex nature and extensive non-linearities of the problem, introduced by the HPA input-output relation, the HPA power consumption model, the phase model of the low-resolution PS, and the EH model.

- We show numerically that the overall power consumption decreases as the DAC/PSs resolution, and antenna length increase, while it increases with the operation frequency.

Structure: Section II introduces the system model, Section III presents the harvested power and the power consumption, and the problem formulation together with the optimization framework is discussed in Section IV. Numerical analysis is provided in Section V, while Section VI concludes the paper.

II. SYSTEM MODEL

We consider an RF-WPT system comprising three key building blocks, i.e., a PT, wireless channel, and ER, as illustrated in Fig. 1. The PT utilizes a uniform planar array (UPA) with half-wavelength spaced radiating elements in the horizontal and vertical directions, represented as H and V , respectively. The total number of antenna elements is given by $N = V \times H$. We consider an analog architecture where the output of a single RF chain is connected to all the radiating elements, which are equipped with PSs.

A. Transmitter

1) *Multi-tone Signal Generation:* Recall that utilizing a multi-tone signal can improve the end-to-end PTE by exploiting non-linearities at the transmitter and receiver [5], [8]. Hence, we consider a signal with K tones and frequency spacing Δ_f between adjacent tones. Thus, the baseband signal bandwidth and baseband frequency of the k th tone is $BW = K\Delta_f$ and $f_k = k\Delta_f$, respectively. An inverse discrete Fourier transform (IDFT) block converts the signal to the time domain. With the sampling frequency \tilde{f}_s and the sampling time $T_s = 1/\tilde{f}_s$, the IDFT for a signal $x(t)$ can be expressed as

$$x(nT_s) = \frac{1}{K} \sum_{k=0}^{K-1} X_k e^{j2\pi f_k nT_s + \phi_k}, n = 0, 1, 2, \dots, \quad (1)$$

where X_k and ϕ_k are the amplitude and phase of the k th tone.

2) *DAC:* We assume a DAC with a resolution of n_b bits and input signal's voltage range $[-A, A]$. Thus, based on (1), we can write $\sum_{k=0}^{K-1} |X_k| \leq A$, while we assume a linear quantization with step size $\Delta = \frac{2A}{2^{n_b}}$. Hereby, $x(t)$ is quantized by rounding it to the nearest value of the quantization step size Δ , i.e., $x^{dac}(t) = \lfloor x(t)/\Delta \rfloor \Delta$.

3) *Low-pass Filter (LPF):* An LPF filters out undesired high frequencies introduced by DAC. The discrete Fourier transform (DFT) of the quantized signal, i.e., $X^{dac} = \text{DFT}\{x^{dac}(t)\}$, is considered for spectrum analysis, while the LPF output is $X^{lpf} = X^{dac}|_{f \leq BW}$.

4) *Mixer:* The mixer upconverts the signal to the desired RF, i.e., f_{ca} , by a local oscillator with its output given by

$$x^{mix}(t) = \Re \{ x^{lpf}(t) e^{j2\pi f_{ca} t} \}, \quad (2)$$

where $x^{lpf}(t)$ is the analog signal at the output of the LPF and $\Re\{\cdot\}$ is the real operator.

5) *HPA:* We employ the Rapp model for solid-state power amplifiers [19] to capture the HPA's non-linear behavior. Hereby, the output signal of the HPA is given by

$$x^{hpa}(t) = G x^{mix}(t) \left(1 + (G |x^{mix}(t)| / A_s)^{2\beta} \right)^{-\frac{1}{2\beta}}, \quad (3)$$

where G represents the amplifier gain, A_s is the saturation voltage, while β is the smoothing parameter of the amplifier.

6) *Transmit Signal:* The RF signal goes through PSs with a finite resolution of B bits for phase adjustment before being fed into the UPA elements. Hence, the signal transmitted by the l th element in the i th row of the UPA is given by

$$x_{i,l}^{UPA}(t) = (1/\sqrt{L_{ps}N}) e^{-i\frac{2\pi b_{i,l}}{2^B}} x^{hpa}(t), \quad (4)$$

where $b_{i,l} \in \{0, 1, \dots, 2^B - 1\}$ is the corresponding quantized phase shift and L_{ps} represents the insertion loss.

B. Channel Model

We consider a near-field channel model [20], which also applies to far-field conditions. Let us proceed by defining the Cartesian coordinates of the l th antenna element in the i th row as $\mathbf{p}_{i,l} = (x_{i,l}, y_{i,l}, z_{i,l})$. Then, the channel coefficient between the ER, located at $\mathbf{p} = (x, y, z)$, and the l th element of the i th row of the UPA corresponding to the k th tone is given as

$$H_{i,l,k} = A_{i,l,k} e^{-\frac{j2\pi}{\lambda_k} \|\mathbf{p} - \mathbf{p}_{i,l}\|_2}. \quad (5)$$

Herein, $\frac{2\pi}{\lambda_k} \|\mathbf{p} - \mathbf{p}_{i,l}\|_2$ is the phase shift caused by the distance traveled by the k th tone from the transmitter to the receiver and λ_k is the wavelength of the k th tone. The corresponding channel gain coefficient is given by [21]

$$A_{i,l,k} = \lambda_k \sqrt{F(\Theta_{i,l})} / (4\pi \|\mathbf{p} - \mathbf{p}_{i,l}\|_2), \quad (6)$$

where $\Theta_{i,l} = (\theta_{i,l}, \psi_{i,l})$ represents the elevation-azimuth pair from the l th element of the i th row of the UPA to the ER. The radiation profile $F(\Theta_{i,l})$ of each element is modeled as [21]

$$F(\Theta_{i,l}) = \begin{cases} 2(b+1) \cos^b(\theta_{i,l}), & \theta_{i,l} \in [0, \pi/2], \\ 0, & \text{otherwise,} \end{cases} \quad (7)$$

where b is the boresight gain. The RF signal at the ER is

$$r^{UPA}(t) = \sum_{i=1}^V \sum_{l=1}^H \sum_{k=0}^{K-1} H_{i,l,k} x_{i,l}^{UPA}(t). \quad (8)$$

C. Energy Receiver

The ER structure, shown in Fig. 2 [6], comprises i) an antenna, equivalently represented as a voltage source connected in series with a resistance, R_s , with $v_s(t) = 2\sqrt{R_s} r^{UPA}(t)$ being the source voltage; ii) an impedance matching network matching the antenna impedance to the impedance of the rectifier circuitry for maximum power delivery; iii) a rectifier converting the RF alternating current (AC) signal received from the antenna into a DC signal used to charge the load. We assume perfect impedance matching, i.e., $R_s = R_{in}$, where R_{in} refers to the input resistance of the rectifier. The

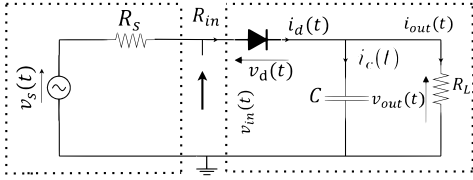


Fig. 2: Antenna equivalent circuit (left) and the rectifier (right).

rectifier includes a single diode and an LPF connected to a load resistance R_L . The LPF is used to filter out any remaining RF signals and noise from the rectified DC output.

The input voltage of the rectenna is given by $v_{in}(t) = \frac{v_s(t)}{2} = \sqrt{R_s} r^{UPA}(t)$, while output voltage is $v_{out}(t) = \bar{v}_{out} + \tilde{v}_{out}(t)$, where \bar{v}_{out} represents the DC component and $\tilde{v}_{out}(t)$ represents the AC component. One can obtain [6]

$$e^{\frac{\bar{v}_{out}}{\eta V_0}} \left(1 + \frac{\bar{v}_{out}}{R_L I_0}\right) = \frac{1}{T} \int_T e^{\frac{\sqrt{R_s} r^{UPA}(t)}{\eta V_0}} dt, \quad (9)$$

where I_0 represents the reverse bias saturation current of the diode, V_0 is its thermal voltage, and η is the ideality factor. Moreover, T represents the integrating period. Finally, the DC power delivered to the load is

$$\bar{p}_{out} = \bar{v}_{out}^2 / R_L. \quad (10)$$

We omit some details here due to space limitations and one can follow [6] for more details.

III. HARVESTED POWER & POWER CONSUMPTION

In this section, we derive the closed-form expression for DC output voltage and formulate the system power consumption.

A. DC Output Voltage

The relationship between the input and output voltages of the rectifier circuit is captured in (9). To proceed further, we rewrite (9) by multiplying its both sides by $\frac{R_L I_0}{\eta V_0} e^{\frac{R_L I_0}{\eta V_0}}$ as

$$\begin{aligned} e^{\left(\frac{\bar{v}_{out} + R_L I_0}{\eta V_0}\right)} \left(\frac{R_L I_0 + \bar{v}_{out}}{\eta V_0}\right) &= \frac{e^{\frac{R_L I_0}{\eta V_0}} R_L I_0}{\eta V_0 T} \int_T e^{\frac{\sqrt{R_s} r^{UPA}(t)}{\eta V_0}} dt \\ \frac{R_L I_0 + \bar{v}_{out}}{\eta V_0} &= W \left(e^{\frac{R_L I_0}{\eta V_0}} \frac{R_L I_0}{\eta V_0 T} \int_T e^{\frac{\sqrt{R_s} r^{UPA}(t)}{\eta V_0}} dt \right) \\ \bar{v}_{out} &= \eta V_0 W \left(e^{\frac{R_L I_0}{\eta V_0}} \frac{R_L I_0}{\eta V_0 T} \int_T e^{\frac{\sqrt{R_s} r^{UPA}(t)}{\eta V_0}} dt \right) - R_L I_0, \end{aligned} \quad (11)$$

where the last line comes from using the product log or Lambert W function $W[\cdot]$. Moreover, the integral in (11) is evaluated by taking the mean of the time domain samples of exponent. Then, \bar{p}_{out} can be obtained using (10).

B. Power Consumption

The overall power consumption of the system is the sum of the power consumed by each component at the transmitter side. Thus, the total power consumption of the system is

$$P_c = P_{dac}(n_b, \tilde{f}_s) + P_{mix} + P_{lo} + P_{hpa} + P_s, \quad (12)$$

where $P_{dac}(n_b, \tilde{f}_s)$ is the power consumed by the n_b -bit DAC functioning with sampling frequency \tilde{f}_s , while P_{hpa} , P_{mix} , and P_{lo} are the power consumed by the HPA, mixer, and local oscillator, respectively. Moreover, $P_s = \frac{1}{K} \sum_{k=0}^{K-1} |X_k|^2$ is the power of the generated signal.

1) *DAC Power Consumption*: The power consumed by the DAC can be written as [11]

$$P_{dac}(n_b, \tilde{f}_s) \approx \alpha [V_{dd} I (2^{n_b} - 1) + C_p \tilde{f}_s V_{dd}^2 n_b] / 2, \quad (13)$$

where V_{dd} is the voltage of the power supply, I is the unit current source that corresponds to the least significant bit, and

C_p is the parasitic capacitance of the switches used to choose the DAC's supported states, while the second-order effects are captured by the correction factor α .

2) *HPA Power Consumption*: The input and output power of HPA is given by $P_{in} = \mathbb{E}(|x^{mix}(t)|^2) / R_{in}$ and $P_{out} = \mathbb{E}(|x^{hpa}(t)|^2) / R_{out}$, respectively, where R_{in} and R_{out} are the input and output resistance of the HPA. The power consumption of the HPA can then be expressed as $P_{hpa} = P_{out} - P_{in}$.

IV. OPTIMIZATION FRAMEWORK

We focus on the joint waveform and beamforming optimization to minimize the power consumption while satisfying the user's DC power requirement, specified by P_{dc} , i.e.,

$$\text{minimize}_{X_k, \phi_k, b_{i,l}} P_c \quad (14a)$$

$$\text{subject to } \bar{p}_{out} \geq P_{dc}. \quad (14b)$$

Note that both (14a) and (14b) are non-convex functions of the optimization variables and deal with extensive non-linearities caused by HPA and rectenna.

A. Waveform and Beamforming Optimization

It is challenging to solve problem (14) directly; thus, we reformulate it as

$$\text{minimize}_{X_k, \phi_k, b_{i,l}} P_c + \Upsilon(P_{dc} - \bar{p}_{out}), \quad (15)$$

which is an unconstrained optimization problem. Moreover, $\Upsilon(x)$ in (15) is an indicator function being ∞ if $x \geq 0$ and 0 otherwise. This indicator function facilitates removing the constraint (14b) and transforming (14) into (15). Hereby, the optimization problem is compelled to discover feasible solutions, leading the second term to become zero, prior to minimizing the power consumption of the system. Note that problem (15) is highly non-linear and non-convex, which can be solved using meta-heuristic algorithms, such as PSO.

PSO is inspired by the social behavior of swarms in nature. It involves a swarm of particles N_p , each representing a potential solution, moving in the solution space. These particles adjust their positions based on their own best experiences \mathbf{p}_{b_i} and those of their neighbors \mathbf{g}_b , leading to convergence towards a solution after a sufficient number of iterations [22]. Moreover, \mathbf{p}_{b_i} is defined as the best position that the i th particle has found during the optimization procedure. Additionally, $\mathbf{g}_b = \xi(\mathbf{z}_i^*)$ is the best objective value in the entire swarm, where ξ is the objective function of the optimization problem.

Let us proceed by defining $\mathcal{S} = \{\mathbf{z}_1, \mathbf{z}_2, \dots, \mathbf{z}_{N_p}\}$ as the swarm set for the optimization problem, where $\mathbf{z}_i = [X_{i,1}^T, \dots, X_{i,K}^T, \phi_{i,1}^T, \dots, \phi_{i,K}^T, b_{i,1}, \dots, b_{i,N}]^T \in \mathbb{R}^{(2K+N) \times 1}$ is the i th particle. Moreover, \mathbf{z}_i denotes the concatenation of the digital beamforming weights amplitude, phase, and variables corresponding to the PSs configurable phases, thus $N_{var} = 2K + N$ is the number of variables. Note that PSO does not handle integer variables and since $b_{i,l}$ is an integer denoting the selected PS phase shift, we define \bar{b} as a continuous variable in $[0, 1]$, and then, compute $b_{i,l}$ using $\bar{b}_{i,l}$ when evaluating the objective function.

Algorithm 1 illustrates the waveform and beamforming design algorithm, which requires several update-evaluate steps to reach a suboptimal solution. First, we generate an initial population of random particles and initialize the parameters. Next, for each particle, (15) is evaluated and \mathbf{p}_{b_i} and \mathbf{g}_b are obtained. Note that the variables corresponding to the phase shifts are continuous in the range $[0, 1]$; thus, this value should be up-scaled and converted to an integer to match the characteristic of the limited-resolution phase shifts, as in line 10. During the update steps (lines 18-19), the next velocity

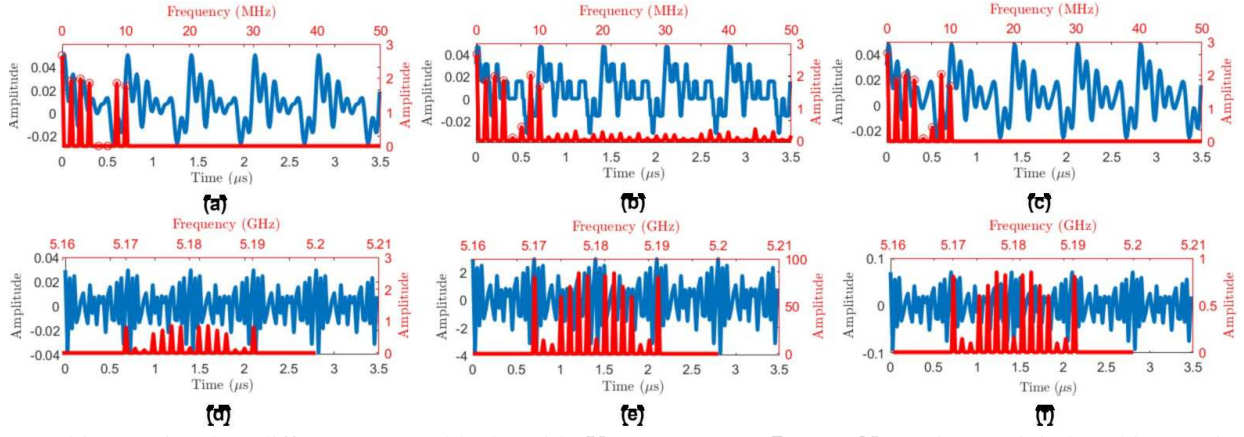


Fig. 3: Multi-tone signal at different system blocks with $K = 8$, $n_b = 2$, $B = 3$, $N = 25$. (a) Digital multi-tone signal, (b) DAC output signal, (c) LPF output signal, (d) mixer output signal, (d) HPA output signal, and (e) RF signal at the ER.

Algorithm 1 PSO-based waveform and Beamforming Design.

```

1: Inputs:  $w, c_1, c_2, I_{max}, N_p, \mathcal{K}, K, N_{var}, B, P_{dc}, X_{max}$ 
2: Outputs:  $P_c, X_k, \phi_k, b_{i,l}$ 
3: Initialize:
4:  $t = 1, v_{i,j} = 0, \mathbf{z}_{min,j} = 0, \forall j$ 
5:  $\mathbf{z}_{max,j} = X_{max}, \text{ for } j = 1, \dots, K$ 
6:  $\mathbf{z}_{max,j} = 2\pi, \text{ for } j = K + 1, \dots, 2K$ 
7:  $\mathbf{z}_{max,j} = 1, \text{ for } j = 2K + 1, \dots, N_{var}$ 
8: Generate random swarm set  $\mathcal{S}$  with  $|\mathcal{S}| = N_p$ 
9: for  $i = 1, \dots, N_p$  do
10:    $b_{i,l} = \lfloor \bar{b}_{i,l}(2^B - 1) \rfloor, \forall l$ 
11:    $\mathbf{p}_{b_i} = \mathbf{z}_i, \mathbf{i}^* = \text{argmax}_i \xi(\mathbf{z}_i), \mathbf{g}_b = \mathbf{z}_i^*$ 
12: end for
13: for  $t = 1, \dots, I_{max}$  do
14:   for  $i = 1, \dots, N_p$  do
15:     for  $j = 1, \dots, N_{var}$  do
16:       Choose  $\mathcal{K} \subset \mathcal{S}$  randomly
17:       Select  $r_1$  and  $r_2$  randomly in  $(0, 1)^{N_{var} \times 1}$ 
18:        $v_{i,j}^t = wv_{i,j}^{t-1} + c_1r_1(\mathbf{p}_{b_i}^{t-1} - \mathbf{z}_{i,j}^{t-1}) + c_2r_2(\mathbf{g}_{b_j}^{t-1} - \mathbf{z}_{i,j}^{t-1})$ 
19:       Update  $\mathbf{z}_{i,j}^t = \mathbf{z}_{i,j}^{t-1} + v_{i,j}^t, b_{i,l} = \lfloor \bar{b}_{i,l}(2^B - 1) \rfloor$ 
20:     end for
21:     if  $\xi(\mathbf{z}_i) < \xi(\mathbf{p}_{b_i})$  then  $\mathbf{p}_{b_i} \leftarrow \mathbf{z}_i$  end if
22:     if  $\xi(\mathbf{z}_i) < \xi(\mathbf{g}_b)$  then  $\mathbf{g}_b \leftarrow \mathbf{z}_i$  end if
23:   end for
24: end for

```

and the position of the particles are updated. Specifically, $v_{i,j}^t$ and $\mathbf{z}_{i,j}^t$ are the velocity and the position of the j th dimension of the i th particle at iteration t , respectively. After that, for each particle, the fitness function is calculated, while the \mathbf{p}_{b_i} of each particle and the \mathbf{g}_b of the swarm are updated (line 19). The procedure is repeated until the maximum number of iterations, i.e., I_{max} , is reached. Notably, the complexity of the algorithm increases with the number of variables, thus, more iterations and swarm size may be needed to attain a proper solution.

PSO has several parameters that can be modified to improve its performance depending on the optimization problem. For instance, w is the inertia weight, which is a balancing factor between exploration and exploitation. Large w offers more

TABLE I: System model parameters.

| Symbol | Value | Ref | Symbol | Value | Ref |
|-----------|-------------|------|----------|----------------|------|
| V_{dd} | 3 V | [11] | A_s | 10 | [16] |
| R_s | 50 Ω | [6] | β | 4 | [16] |
| L_{ps} | 0.5 dB | [24] | R_L | 1.6 K Ω | [6] |
| P_{mix} | 23 mW | [25] | A | 1 V | [11] |
| I_0 | 5 μ A | [6] | P_{lo} | 5 mW | [25] |
| V_0 | 25.86 mV | [6] | G | 10 | [10] |
| α | 1 | [11] | η | 1.05 | [6] |
| C_p | 1 pF | [11] | I | 10 μ A | [11] |

For simplicity, we have used $R_{in} = R_{out} = 1 \Omega$. In practice, these values would depend on the design of the HPA.

exploration, while smaller w facilitates more exploitation. Moreover, c_1 and c_2 are the weights for personal experience and social interaction. Additionally, \mathbf{z}_{min} and \mathbf{z}_{max} are N_{var} -dimensional vectors denoting the lower and upper bound of the optimization variables, respectively.

B. Complexity Analysis

The complexity of Algorithm 1 is determined by the computation complexity of (15) and the intricacy of the PSO. The bottleneck of this process is the computation time of \bar{v}_{out} , which scales with K, N , the number of time samples in the charging period, i.e., N_{tp} , and IDFT computational complexity, i.e., $\mathcal{O}(K \log K)$, as seen in (1) and (8). Therefore, the complexity of calculating \bar{v}_{out} is $\mathcal{O}(K^2 N N_{tp} \log K)$. Since the process is repeated for all particles, the total complexity of the utilized PSO algorithm is $\mathcal{O}(N_p K^2 N N_{tp} \log K)$.

V. NUMERICAL ANALYSIS

We consider the ER is located at 3 m distance in the boresight direction of the UPA with an EH requirement of $P_{dc} = 20 \mu$ W [23]. The array is square-shaped with $V = \frac{H}{\sqrt{N}}$, while we set $X_{max} = 300$ V, $BW = 10$ MHz, $f_s = 100$ MHz, and $f_{ca} = 5.18$ GHz unless otherwise stated [16]. The rest of the parameters are listed in Table I.

Fig. 3 illustrates the multi-tone signal waveform in time and frequency domains after passing through system blocks. In Fig. 3 (a) and (b), the effect of low-resolution DAC on the signal can be seen, which generates high out-of-band frequencies. Moreover, it can be observed in Fig. 3 (c)-(e) that the frequency response above BW in baseband and outside $[f_{ca} - BW, f_{ca} + BW]$ is zero. Fig. 4 showcases the normalized P_c in the area. As expected, the P_c increases as we move

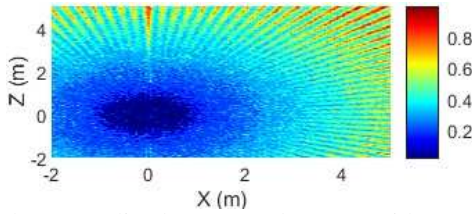


Fig. 4: The normalized consumed power with respect to the path loss for different ER positions in the area.

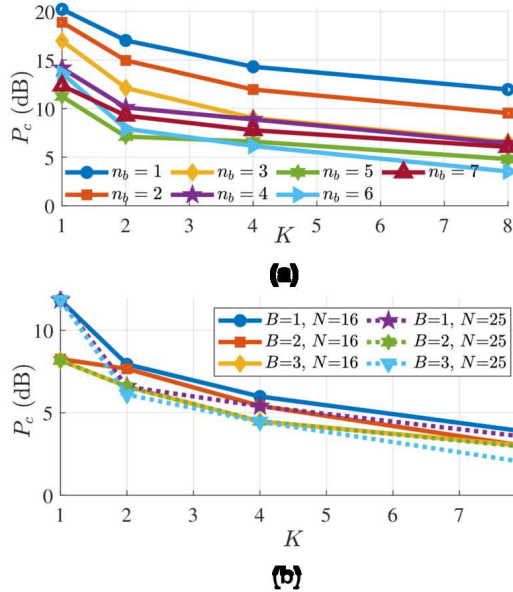


Fig. 5: Power consumption versus K for (a) different n_b values (b) different B and N .

toward further distances from the transmitter, while it is seen that some spatial directions are more power-consuming.

Fig. 5 (a) showcases P_c as a function of K for different DAC resolutions. It is seen that increasing n_b leads to reducing P_c , which is due to better waveform and beamforming capability. Note that at some point using more bits, e.g., $n_b \geq 7$, P_{dac} drastically increases while the waveform/beamforming gains become marginal, which leads to an increase in overall system P_c . Fig. 5 (b) shows P_c versus K for different B and N . It can be observed that the performance is improved by using higher B for PSs, which allows for more control over the direction and shape of the transmitted signal, leading to achieving more harvested power with less power consumption. Finally, Fig. 6 illustrates P_c increasing with f_{ca} for different N . It can be also observed that increasing N leads to reducing P_c . Moreover, the efficiency of HPA tends to decrease at higher frequencies. This is because HPA faces greater challenges in maintaining linearity due to increased parasitic effects, leading to more required input power to achieve the same output power levels.

VI. CONCLUSION

In this paper, we considered a single-user multi-antenna analog RF-WPT system. We first formulated a joint waveform and beamforming optimization aiming to minimize the system power consumption while meeting EH requirements. Then, we proposed an optimization approach relying on PSO to solve the problem. The results evinced that the power consumption decreases as the DAC/PSs resolution and antenna length increase, while increasing frequency leads to larger power consumption. In future studies, we may investigate the performance of the system in multi-user scenarios and the impact of digital/hybrid transmit antenna architectures.

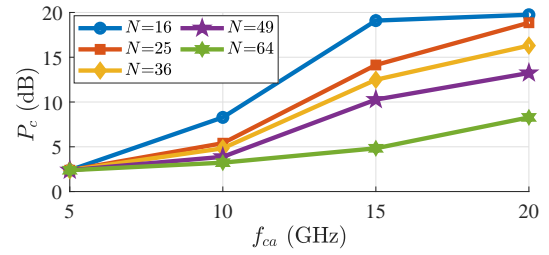


Fig. 6: Power consumption versus the operating frequency for different N values, $K = 8$, $n_b = 3$, and $B = 3$.

REFERENCES

- [1] O. López *et al.*, “Massive Wireless Energy Transfer: Enabling Sustainable IoT Toward 6G Era,” *IEEE Internet Things J.*, vol. 8, no. 11, pp. 8816–8835, 2023.
- [2] O. López *et al.*, “High-power and safe RF wireless charging: Cautious deployment and operation,” *arXiv preprint arXiv:2311.12809*, 2023.
- [3] —, “Zero-energy Devices for 6G: Technical Enablers at a Glance,” *arXiv preprint arXiv:2402.09244*, 2024.
- [4] C. Song *et al.*, “Advances in wirelessly powered backscatter communications: From antenna/RF circuitry design to printed flexible electronics,” *Proc. IEEE.*, vol. 110, no. 1, pp. 171–192, 2021.
- [5] Y. Zeng, B. Clerckx, and R. Zhang, “Communications and signals design for wireless power transmission,” *IEEE Trans. Commun.*, vol. 65, no. 5, pp. 2264–2290, 2017.
- [6] M. R. V. Moghadam, Y. Zeng, and R. Zhang, “Waveform optimization for radio-frequency wireless power transfer,” in *Proc. IEEE SPAWC*, 2017, pp. 1–6.
- [7] A. Azarbahram *et al.*, “Energy Beamforming for RF Wireless Power Transfer with Dynamic Metasurface Antennas,” *IEEE Wirel. Commun. Lett.*, 2023.
- [8] B. Clerckx *et al.*, “Fundamentals of wireless information and power transfer: From RF energy harvester models to signal and system designs,” *IEEE J. Sel. Areas Commun.*, vol. 37, no. 1, pp. 4–33, 2018.
- [9] O. M. Rosabal *et al.*, “Sustainable RF Wireless Energy Transfer for Massive IoT: Enablers and Challenges,” *IEEE Access*, vol. 11, pp. 133 979–133 992, 2023.
- [10] J. Joung *et al.*, “A survey on power-amplifier-centric techniques for spectrum-and energy-efficient wireless communications,” *IEEE Commun. Surv. & Tut.*, vol. 17, no. 1, pp. 315–333, 2014.
- [11] S. Cui, A. J. Goldsmith, and A. Bahai, “Energy-constrained modulation optimization,” *IEEE Trans. Wireless Commun.*, vol. 4, no. 5, pp. 2349–2360, 2005.
- [12] M. Kalcher, M. Fulde, and D. Gruber, “Fully-digital transmitter architectures and circuits for the next generation of wireless communications,” *ELEKTROTECHNIK UND INFORMATIONSTECHNIK*, vol. 135, no. 1, pp. 89–98, 2018.
- [13] I. Ahmed *et al.*, “A survey on hybrid beamforming techniques in 5G: Architecture and system model perspectives,” *IEEE Commun. Surv. & Tut.*, vol. 20, no. 4, pp. 3060–3097, 2018.
- [14] B. Clerckx *et al.*, “Waveform design for wireless power transfer,” *IEEE Trans. Signal Process.*, vol. 64, no. 23, pp. 6313–6328, 2016.
- [15] S. Shen and B. Clerckx, “Joint waveform and beamforming optimization for MIMO wireless power transfer,” *IEEE Trans. Commun.*, vol. 69, no. 8, pp. 5441–5455, 2021.
- [16] Y. Zhang and B. Clerckx, “Waveform design for wireless power transfer with power amplifier and energy harvester non-linearities,” *IEEE Trans. Signal Process.*, 2023.
- [17] Z. Feng, B. Clerckx, and Y. Zhao, “Waveform and beamforming design for intelligent reflecting surface aided wireless power transfer: Single-user and multi-user solutions,” *IEEE Trans. Wireless Commun.*, vol. 21, no. 7, pp. 5346–5361, 2022.
- [18] A. Azarbahram *et al.*, “Waveform optimization and beam focusing for near-field wireless power transfer with dynamic metasurface antennas and non-linear energy harvesters,” *arXiv:2307.01081*, 2024.
- [19] C. Rapp, “Effects of HPA-nonlinearity on a 4-DPSK/OFDM-signal for a digital sound broadcasting signal,” *ESA Spec. Publ.*, vol. 332, pp. 179–184, 1991.
- [20] H. Zhang *et al.*, “Beam focusing for near-field multiuser MIMO communications,” *IEEE Trans. Wireless Commun.*, vol. 21, no. 9, pp. 7476–7490, 2022.
- [21] S. W. Ellingson, “Path loss in reconfigurable intelligent surface-enabled channels,” in *Proc. IEEE PIMRC*, 2021, pp. 829–835.
- [22] J. Kennedy and R. Eberhart, “Particle swarm optimization,” in *Proc. ICNN’95-Int. Conf. Neural Netw.*, vol. 4. IEEE, 1995, pp. 1942–1948.
- [23] B. Clerckx and J. Kim, “On the beneficial roles of fading and transmit diversity in wireless power transfer with nonlinear energy harvesting,” *IEEE Trans. Wireless Commun.*, vol. 17, no. 11, pp. 7731–7743, 2018.
- [24] J. Eisenbeis *et al.*, “Comparison of hybrid beamforming systems using phase shifters and switches,” in *GeMiC*. IEEE, 2019, pp. 40–43.
- [25] C. Lin and G. Y. Li, “Energy-efficient design of indoor mmWave and sub-THz systems with antenna arrays,” *IEEE Trans. Wireless Commun.*, vol. 15, no. 7, pp. 4660–4672, 2016.